Integrating quantum dots and dielectric mie resonators: A hierarchical metamaterial inheriting the best of both

Capretti, A.; Lesage, A.; Gregorkiewicz, T.

DOI
10.1021/acsphotonics.7b00320

Publication date
2017

Document Version
Final published version

Published in
ACS Photonics

ACS Photonics

Article

Cite This: ACS Photonics 2017, 4, 2187-2196

pubs.acs.org/journal/apchd5

Integrating Quantum Dots and Dielectric Mie Resonators: A Hierarchical Metamaterial Inheriting the Best of Both

Antonio Capretti,* Arnon Lesage, and Tom Gregorkiewicz

University of Amsterdam, Science Park 904, 1098XH Amsterdam, The Netherlands

Supporting Information

ABSTRACT: Nanoscale dielectric resonators and quantum-confined semiconductors have enabled unprecedented control over light absorption and excited charges, respectively. In this work, we embed luminescent silicon nanocrystals (Si-NCs) into a 2D array of SiO_2 nanocylinders and experimentally prove a powerful concept: the resulting metamaterial preserves the radiative properties of the Si-NCs and inherits the spectrally selective absorption properties of the nanocylinders. This hierarchical approach provides increased photoluminescence (PL) intensity obtained without utilizing any lossy plasmonic components. We perform rigorous calculations and predict that a freestanding metamaterial enables tunable absorption peaks up to 50% in the visible spectrum, in correspondence with the nanocylinder Mie resonances and of the grating condition in the array. We experimentally detect extinction spectral peaks in the metamaterial, which drive enhanced absorption in the Si-NCs. Consequently, the metamaterial features increased PL intensity, obtained without affecting the PL lifetime, angular pattern, and extraction efficiency. Remarkably, our best-performing metamaterial shows +30% PL intensity achieved with a lower amount of Si-NCs, compared to an equivalent planar film without nanocylinders, resulting in a 3-fold average PL enhancement per Si-NC. The principle demonstrated here is general, and the Si-NCs can be replaced with other semiconductor quantum dots, rare-earth ions, or organic molecules. Similarly, the dielectric medium can be adjusted on purpose. This spectral selectivity of absorption paves the way for an effective light down-conversion scheme to increase the efficiency of solar cells. We envision the use of this hierarchical design for other efficient photovoltaic, photocatalytic, and artificial photosynthetic devices with spectrally selective absorption and enhanced efficiency.

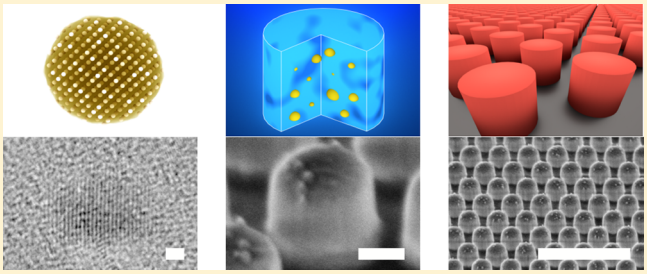

KEYWORDS: *dielectric metamaterial, hierarchical metamaterial, Mie resonator, silicon nanocrystal, quantum dot*

Nanoscale solid-state systems are boosting the prospects of material science by providing unparalleled optical and electronic functionalities. Semiconductors with size comparable to or smaller than the exciton Bohr radius (a few nanometers), such as quantum dots and nanowires, display quantum-confinement properties. The confinement of the electron wave function determines the quantization of the energy states, accompanied by the widening of the semiconductor band gap, the increase of radiative recombination, and the onset of carrier multiplication.[1−3] A number of pioneering works have investigated the interplay between plasmonic resonators and quantum dots, showing that this interaction features enhanced absorption and emission rate.[4−6] Unfortunately, plasmonic resonances come with large parasitic losses, heating due to dissipation in the metal, and incompatibility with CMOS fabrication technology.[7−9] These drawbacks are particularly detrimental for energy-related and -sustainable applications, which require technological solutions excluding lossy metals and expensive/toxic semiconductors.

On the other hand, high-index dielectric nanoparticles with size of hundreds of nanometers support Mie resonances without utilizing metal components.[10,11] Differently from plasmonic nanoparticles, whose scattering is dominated by electric modes, their resonances are both magnetic and electric in nature, with comparable strengths.[8,9,12] For refractive indices of >2, available with group IV and group III−V semiconductors, dipole and quadrupole resonant modes are well-defined.[9] Moreover, they guarantee reduced optical losses with respect to their plasmonic counterpart.[7−9] Interference effects between magnetic and electric dipole modes have been shown to enable directional light scattering, as well as scattering suppression.[13,14] Building on the spectrally selective optical properties of the dielectric scatterers,[12,15] dielectric metamaterials have been very recently investigated for controlling the transmission/reflection ratio in the infrared,[16] for light concentration to an absorbing substrate,[17] for nonlinear optical applications,[18] and for flat optics[19,20] and are currently being explored for photovoltaics.[21,22]

Here, we explore the opportunity to combine quantum dots and dielectric resonators as building blocks of a hierarchical metamaterial, which not only inherits the intrinsic optical and electronic properties of its nanoscale constituents but also features enhanced performance. This simple yet powerful

Received: March 29, 2017
Published: August 3, 2017

DOI: 10.1021/acsphotonics.7b00320
ACS Photonics 2017, 4, 2187−2196

scheme is of great impact for applications in photovoltaics, photocatalysis, and artificial photosynthesis, as well as for increasing the sustainability of the available optoelectronic devices. In this work, we integrate quantum-confined luminescent silicon nanocrystals (Si-NCs) within SiO_2 nanocylinders, arranged in a 2D array as depicted in Figure 1a–c.

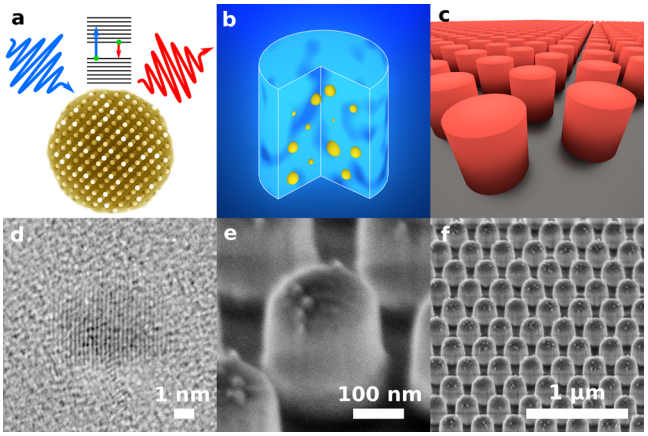

Figure 1. Schematic of the hierarchical metamaterial: (a) quantum-confined Si-NCs, (b) SiO_2 nanocylinders resonating at the excitation wavelength, and (c) photoluminescent 2D planar array. (d) HRTEM of a Si-NC in a SiO_2 matrix, (e) SEM of a SiO_2 nanocylinder with a height of 300 nm and diameter of 215 nm, and (f) SEM of the 2D metamaterial. Scale bars for panels (d)–(f) are 1 nm, 100 nm, and 1 μm, respectively.

We demonstrate that the resulting metamaterial preserves the radiative recombination properties of the Si-NCs, inherits the spectrally selective absorption of the nanocylinder array, and features enhanced emission intensity. As a proof of concept, we tackle the spectral requirements of a light down-converter for solar cells,[23] namely, (i) total absorption of photons with energy $E > 2E_{gap}$ and (ii) total transmission of photons with $E < 2E_{gap}$, where E_{gap} is the cell band gap ($E_{gap} \approx 1.11$ eV for Si). We address these requirements by designing a hierarchical metamaterial optimized on three levels:

(a) Si-NCs are quantum dots made of crystalline Si (see HRTEM in Figure 1d) with a typical diameter of <10 nm. The electron wave function is broadened in the momentum space due to the Heisenberg uncertainty principle, increasing the rate of radiative recombination. Therefore, the constraint of momentum conservation is relaxed (Si is an indirect semiconductor) and Si-NCs show excitonic photoluminescence (PL) in the red/infrared spectrum.[3,24] Notably, the occurrence of carrier multiplication in ensembles of Si-NCs, due to a process named space-separated quantum cutting (SSQC),[25,26] enables the down-conversion of one high-energy photon into two photons with half of the original energy. This has the huge potential to enable sunlight spectral shaping and to truly improve the efficiency of solar cells by down-conversion.[23,27−29]

(b) The dielectric nanocylinders, shown in the SEM of Figure 1e, are made of a solid-state dispersion of Si-NCs in a SiO_2 matrix (Si-NC:SiO_2, in brief) and defined by electron-beam lithography. The average size of the Si-NCs (~2.6 nm) is 2 orders of magnitude smaller than the wavelength of visible light, and, therefore, Si-NC:SiO_2 is effectively a homogeneous medium. The effective refractive index n_{eff} is a function of the volume fraction of Si-NCs, and it is $n_{eff} \approx 1.9$ for the samples produced in this work (see Methods section). The excellent scattering properties of the nanocylinders depend on their size, shape, and high refractive index n_{eff}, enabling the onset of Mie resonances in the visible spectrum.[17,21,22]

(c) The 2D hexagonal array of scattering nanocylinders forms an optically thin metamaterial, as shown in Figure 1f, with enhanced absorption properties. Superabsorption in a thin 1D dielectric metamaterial has been recently shown to arise from the interference between the scattered and the incident waves, which enables an optimal match of the optical impedances.[30] This results in a maximum absorption of 50% for freestanding dielectric metamaterials, like their metal counterpart, and 100% absorption with the support of a back-reflector.

In the following, we experimentally demonstrate that the investigated metamaterial supports extinction peaks in correspondence with the nanocylinder Mie resonances and the grating condition of the array, whose spectral positions are tailored by geometrical design parameters. Our numerical predictions show that the metamaterial absorption can reach up to 50%. The optical losses in SiO_2 are negligible in the visible spectrum, and, therefore, the main contribution to the absorption comes from optical transitions in the Si-NCs. We experimentally prove that the increased absorption directly couples to the Si-NCs, resulting in a 3-fold average PL enhancement per Si-NC. Specifically, our experiments indicate that the PL intensity from the best performing metamaterial is +30% compared to a planar Si-NC:SiO_2 film (without the nanocylinder patterning), despite that the number of photoluminescent Si-NCs is reduced to 43%.

The investigated metamaterial can find application as an optically thin down-converter of light on the front surface of commercial solar cells. It is fair to remark that this application necessarily requires a PL quantum yield (QY) above 50%, while the maximum value achieved so far for Si-NC:SiO_2 is 35%.[31] A flourishing and growing field of research is tackling the increase of QY to match the requirements for applications.[31,32] Nevertheless, the fundamental goal of this work is to demonstrate that the integration of quantum emitters into dielectric resonators enables spectrally selective enhancement of photon absorption, obtained without affecting the emitter radiative properties and resulting in an overall increase of PL intensity. Although we propose and use a specific material platform, the demonstrated principle is general and can be applied to other semiconductor quantum dots and emitting species, such as rare-earth ions and organic molecules. We envision the application of this principle to areas such as light conversion and spectral shaping for photovoltaics, but also photocatalysis and artificial photosynthesis.

METHODS

In the deposited Si-NC:SiO_2 films, the size of Si-NCs is 2 orders of magnitude smaller than the wavelength of visible light and their volume fraction f is 17 ± 4%. Therefore, Si-NC:SiO_2 can be effectively approximated as a homogeneous medium, with intermediate optical properties between Si and SiO_2. Detailed studies of the refractive index of Si-NC:SiO_2 films can be found in the literature,[33,34] showing that its value approaches 1.9 for the stoichiometry of interest in our work (SiO_x with $x \approx 1.37$) and that there is good agreement with the Maxwell–Garnett formula.[35] Small deviations are due to the fact that the electronic states of Si-NCs are strongly affected by quantum confinement, and therefore the NC refractive index is different from bulk Si. We apply the Maxwell–Garnett homogenization

DOI: 10.1021/acsphotonics.7b00320
ACS Photonics 2017, 4, 2187–2196

formula to estimate the effective refractive index n_{eff}, as shown in Supporting Figure S1, and we find a good agreement with the measured transmission and reflection data. The volume fraction f affects both the optical and electronic properties of the Si-NC:SiO_2 medium. Any change of f modifies the effective refractive index according to the homogenization models: as the concentration of Si increases, the refractive index becomes higher. Moreover, as f increases, the average distance between the Si-NCs is reduced and the probability of SSQC increases as well. Our group demonstrated the existence of an optimal distance for the probability of the SSQC process.[36] Furthermore, the Si-NC size has a strong influence on the PL QY, and an optimum size exists.[31] Therefore, the interplay between f, the deposition parameters, and the film thickness determines the resulting PL spectrum, QY, and SSQC efficiency.[37,38]

We fabricate three sets of metamaterials with nominal nanocylinder height H = 100, 300, and 450 nm. For each height, we produce (on the same substrate) six arrays with nanocylinder diameter from D = 164 to 420 nm. A complete list of investigated samples is provided in the Supporting Table S1. In order to have a fair comparison between metamaterials with the same height, we keep the number of Si-NCs equal in all the metamaterial geometries by fixing the nanocylinder area coverage (AC ≈ 43%). This choice also determines the array spacing. Moreover, all the samples with the same height, including the planar film used as reference, are made starting from the same deposited Si-NC:SiO_2 film, and therefore the optical and electronic properties are the same. The fabrication process consists of a sequence of eight steps (a–h), as illustrated in Supporting Figure S2. First, we deposit a planar film made of Si-NC:SiO_2 with thickness H = 100, 300, and 450 nm (on three different substrates, steps a–c). Then, a nanolithographic method is used to pattern the metamaterial geometry into the Si-NC:SiO_2 films (steps d–h). The fabrication process results in hexagonal 2D arrays of Si-NC:SiO_2 nanocylinders. The arrays have a size of 30 μm. The resulting height H of the nanocylinders is equal to the thickness of the original film deposited in steps a–c.

The optical extinction is measured in a Zeiss Axio Observer inverted microscope. The light source is a halogen lamp focused by a condenser with numerical aperture NA = 0.35, and the transmitted light is collected through a NA = 0.75 100× objective. The spectra are recorded by a Princeton Instruments Acton SpectraPro SP2300 spectrometer equipped with a PyLoN:400 (1340 × 400) cryogenically cooled charge-coupled device (CCD). For the 0th-order extinction, we use a customized system where the light source is a fiber-coupled lamp focused by a NA = 0.42 lens. The transmitted and reflected light beams are collected by identical lenses (for the reflection we additionally use a half transparent mirror) and delivered to an OceanOptics USB2000+Vis-NIR spectrometer. The PL experiments are performed in the same Zeiss Axio Observer inverted microscope. The excitation is the 488 nm line of a Spectra-Physics Stabilite 2017 Ar laser, focused onto a fixed spot of 50 μm by a 100× objective with NA = 0.75. The excitation power is fixed at 2.5 mW. The PL signal is collected by the same objective by using a dichroic mirror and measured by the spectrometer and the CCD camera. The values reported here are the PL intensities integrated across the emission spectrum. For the PL excitation experiment, we use the 415–537.5 nm signal of a SOLAR LP603-I optical parametric oscillator (OPO), pumped by the third harmonic of a Nd:YAG LQ629-10 1064 nm laser with 100 Hz repetition rate and 12 ns pulse duration. The OPO signal is collimated and coupled to the inverted microscope, exciting the samples perpendicularly to their surface. For the PL lifetime measurements, we use the CW output at 445 nm of a Becker & Hickl diode laser, modulated by a square wave with 1 kHz frequency, 100 μs ON-state, and 3 μs fall time.[39] The detector is an ID100 Quantique silicon avalanche photodiode with 40 ps timing resolution, connected to a DPC-230 Becker & Hickl timing card. Absolute QY measurements are performed for the planar Si-NC:SiO_2 films before nanopatterning. The samples are placed in an integrating sphere (7.5 cm in diameter, Newport) with the PL directed into a Solar LS M266 spectrometer coupled with a Hamamatsu S7031-1108S Vis-CCD camera. For excitation, we used a 150 W Hamamatsu L2273 xenon lamp coupled to double grating Solar MSA130 monochromator. The measured QY is ∼2%, while the maximum value achieved so far in the literature is 35%,[31] which requires a time-consuming optimization of the material deposition process (the absolute value of the QY is not relevant for the concept demonstrated in this article). The home-built Fourier microscopy setup consists of a 100× objective with NA = 0.90, a set of telescope lenses L1 and L2 with equal focal lengths (f = 20 mm), and a Fourier lens L3 (f = 200 mm). The detector is an Andor Technology silicon CCD. The excitation is a PicoQuant LDH diode laser at 450 nm, and a pinhole is used to selectively excite one metamaterial sample per each acquisition.

We use the transition matrix method, also known as null-field, to calculate the scattering cross-section spectra of individual nanocylinders.[40] In this method, the expansion coefficients for the scattered field are retrieved by combining the null-field equation with the boundary conditions. We also use the rigorous coupled wave approach (RCWA), also known as the Fourier modal method, to calculate the transmission (T), reflection (R), and absorption (A) spectra of the 2D arrays of nanocylinders.[41] This method is particularly suitable for simulating light interaction with periodic layered structures that are invariant in the direction normal to the periodicity, due to its Fourier basis representation. Under the conditions of perfectly planar films and periodic arrays in the metamaterial regime (when the incident wavelength is larger than the lattice spacing), only the 0th-order transmittance T_0 and reflectance R_0 exist, and therefore we have $T_0 + R_0 + A = 1$. In transmission experiments, the extinction is the fraction of incident light that does not reach the detector, defined as Ext = $1 - T_0$, and therefore Ext = $R_0 + A$. For real films and metamaterials with surface roughness and geometrical imperfections, diffuse (i.e., nondirectional) scattering is also present, both transmitted toward the side of the transmission (T_{ds}) and to the side of the reflection. Therefore, the actual transmittance measured in a transmission experiment is $T = T_0 + T_{ds}$ and Ext = $1 - T = 1 - T_0 - T_{ds}$. Given the diffuse character of T_{ds}, its contribution strongly varies with the angular aperture of the collection optics. For sufficiently narrow apertures we have Ext ≈ $1 - T_0$. Analogous considerations hold for the reflectance R.

For periodic metamaterials in the grating regime (when the incident wavelength is equal to or shorter than the lattice spacing), highly directional diffraction modes take place both in transmission and in reflection. In our RCWA calculations, the total transmittance T and reflectance R take into account all the diffraction modes of any order, including the 0th: $T = T_0 + T_{\pm1} + \cdots + T_{\pm n}$ and $R = R_0 + R_{\pm1} + \cdots + R_{\pm n}$. In these calculations, the diffuse scattering is zero because a perfect periodic

DOI: 10.1021/acsphotonics.7b00320
ACS Photonics 2017, 4, 2187–2196

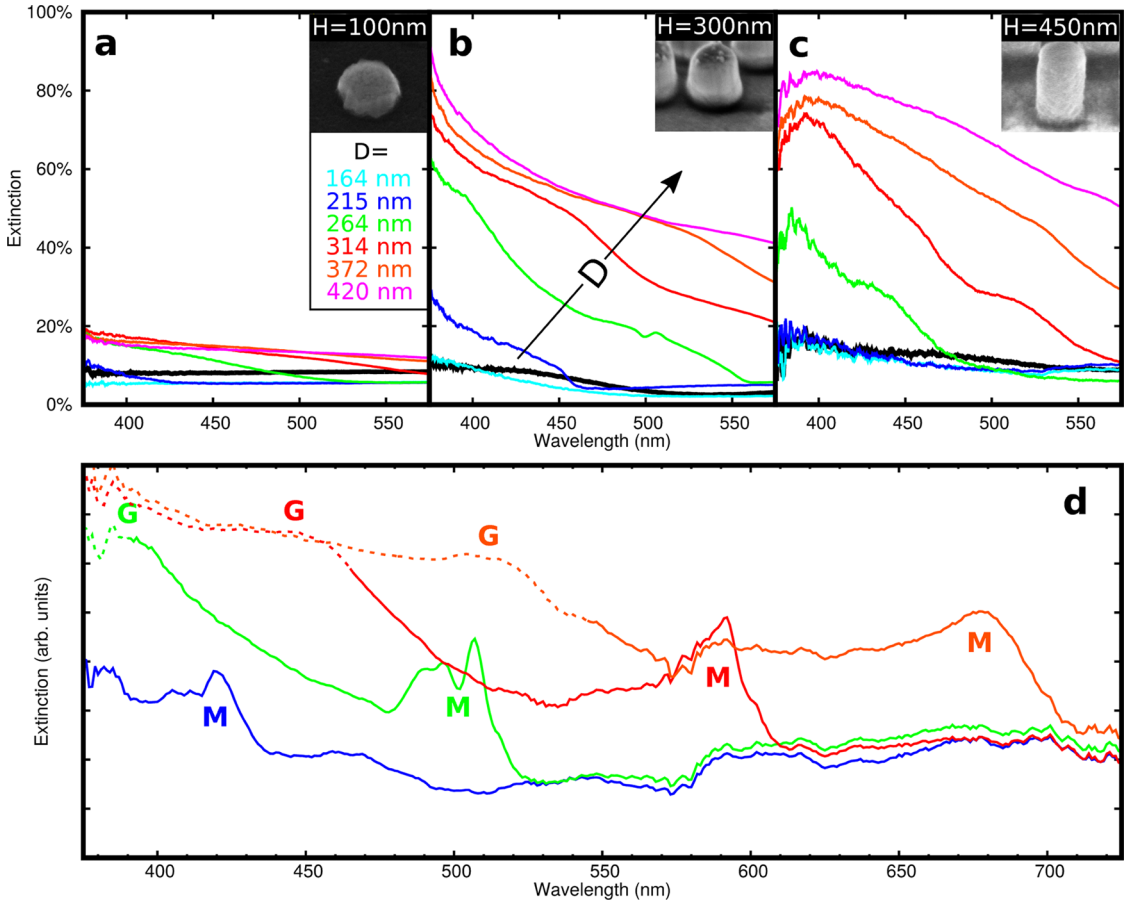

Figure 2. Extinction spectra (collection aperture ±49°) of metamaterials with nanocylinder height (a) H = 100 nm, (b) 300 nm, and (c) 450 nm, parametrized for a diameter in the range 164−420 nm. The spectra of the reference planar films are reported in black for each thickness H. The insets show representative SEMs of the nanocylinder for each height. (d) 0th-order extinction spectra (collection aperture ±25°) of metamaterials with H = 300 nm, parametrized for a diameter from D = 215 to 372 nm. The continuous (dashed) part of the spectra indicates that the wavelength is longer (shorter) than the array spacing.

geometry (in terms of periodicity and unit cell shape) is assumed. Therefore, the absorption is $A = 1 - T - R$.

RESULTS AND DISCUSSION

The metamaterial transmission, scattering, and absorption depend on the nanocylinder size and distance. We quantify this dependence by measuring the extinction spectra in the 350−600 nm spectral range, as shown in Figure 2a−c for the nanocylinder height H = 100, 300, and 450 nm. The extinction is defined as $1 - T$, with T being the transmittance collected with an angular aperture ±49°, which comprises also significant contributions from diffuse scattering (see Methods). The extinction spectra of the three planar Si-NC:SiO_2 films are conveniently reported in black and are used as reference samples throughout this article. For very thin metamaterials (H = 100 nm, Figure 2a), an extinction band appears with increasing diameter D, and the amplitude increases from 5% to only 20% at $\lambda \approx 400$ nm. For metamaterials with H = 300 nm (Figure 2b), the maximum extinction amplitude is boosted up to 70%. In particular, for diameters from 215 to 372 nm, we can distinguish the occurrence of broad extinction peaks in the spectra. These spectra confirm that the nanocylinders with a height of approximately 300 nm are efficient Mie scatterers, whose modes rely on significant retardation effects along the propagation direction. Eventually, if we further increase the metamaterials height to H = 450 nm (Figure 2c), we observe a slight increase with respect to the previous height and a shift in the extinction spectral features, in agreement with previous numerical studies.[17]

To shed light on the origin of the observed spectral features, we focus on the metamaterials with H = 300 nm and measure the 0th-order extinction by narrowing the collection angular aperture to ±25° to reduce the contribution of diffuse scattering. The spectra, shown in Figure 2d, feature neat maxima, whose spectral position spans a wide range from λ = 400 to 700 nm, depending on the nanocylinder diameter. We can easily attribute them to the occurrence of dipole Mie resonances in the nanocylinders. According to a simple rule-of-thumb formula, electric and magnetic dipole resonances appear close in the spectrum, approximately at the wavelength[9−11]

$$\lambda_{\mathrm{Mie,dipole}} = n_{\mathrm{eff}} D \tag{1}$$

In resonators with similar refractive index, the magnetic resonance has been predicted to have a slightly larger wavelength than the electric one.[17] Moreover, the electric mode is expected to red-shift more quickly than the magnetic one by increasing the nanocylinder size.[16] In our measurements, we observe a pronounced peak asymmetry for all the investigated metamaterials and even a double peak for the case D = 264 nm. In addition, we observe extinction maxima occurring at shorter wavelengths than the Mie resonances. Their spectral position approximately coincides with the array

DOI: 10.1021/acsphotonics.7b00320
ACS Photonics 2017, 4, 2187−2196

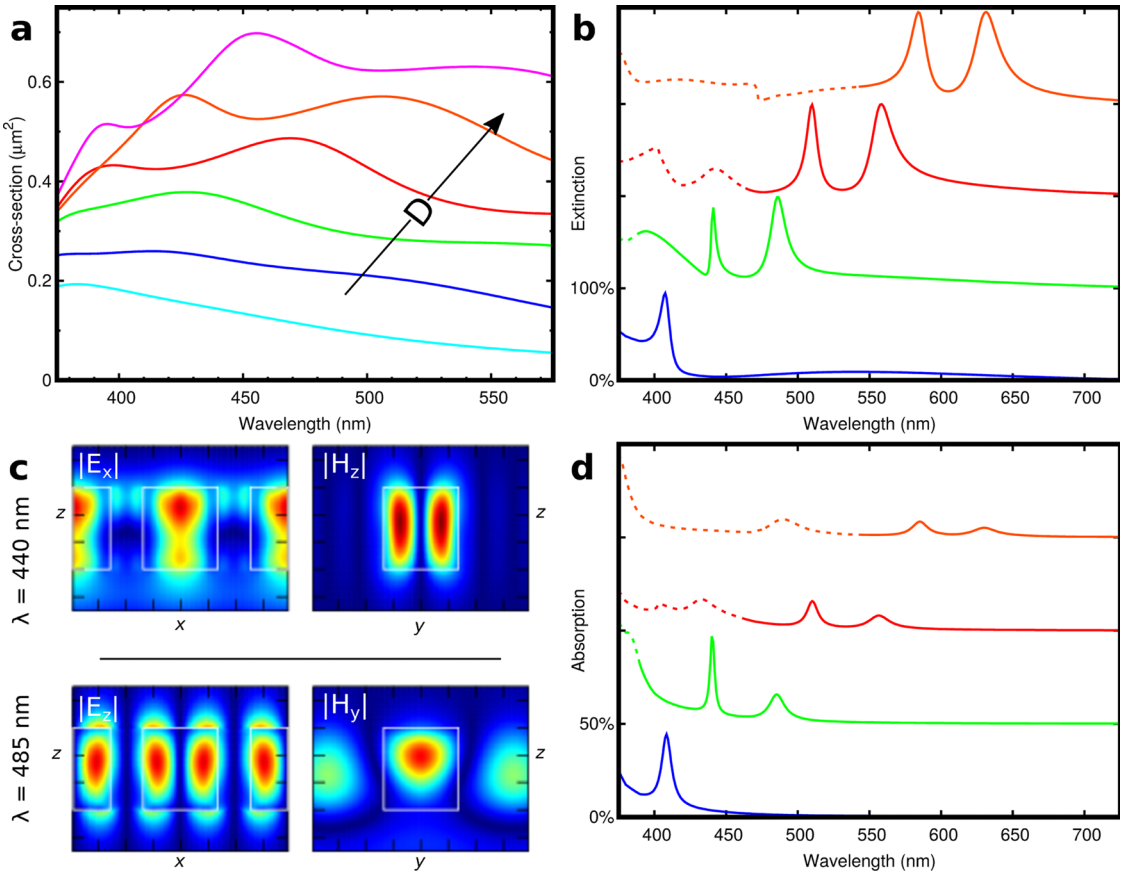

Figure 3. (a) Calculated scattering cross-section spectra of isolated nanocylinders parametrized for the diameter D = 164 nm (cyan), 215 nm (blue), 264 nm (green), 314 nm (red), 372 nm (orange), and 420 (magenta). (b) Calculated extinction spectra of a 2D array of nanocylinders parametrized for the diameter D (colors as in panel a). (c) Electric (left) and magnetic (right) field distributions for the metamaterial with D = 264 nm excited at λ_{exc} = 440 nm (top) and 485 nm (bottom). (d) Same as panel (b) for absorption spectra. All the calculations are relative to nanocylinders with height H = 300 nm.

spacing S, revealing the fact that they are related to the grating condition

$$\lambda_{grating} = S \tag{2}$$

We conclude that our 2D metamaterial design supports extinction peaks due to the occurrence of Mie resonances of the nanocylinders and due to the grating condition. Their spectral position is separate and can be independently tuned by the nanocylinder shape (mainly the diameter) and the array spacing.

To better interpret the difference between the measured extinction spectra of Figure 2b and d, we perform rigorous full-wave electromagnetic calculations of individual (i.e., isolated) nanocylinders and 2D hexagonal arrays. The scattering spectra of individual nanocylinders with H = 300 nm are shown in Figure 3a and are characterized by broadband features, with local maxima shifting as the nanocylinder diameter increases. On the other hand, the calculated extinction spectra $(1 - T)$ for 2D arrays of nanocylinders are shown in Figure 3b, and we can clearly distinguish sharp extinction peaks due to dipole Mie resonances and grating modes. These calculations indicate that the extinction measurements of Figure 2b are dominated by diffuse scattering from the nanocylinders, while the peaks in the spectra of Figure 2d are due to collective resonant modes (this difference is simply obtained by reducing the angular aperture of the detection optics). The identification of the resonances modes in the calculations for 2D arrays can be made by calculating the spatial distribution of the electromagnetic field. As an example, in Figure 3c we show the electric and magnetic fields for the metamaterial with D = 264 nm excited at λ_{exc} = 440 nm (top) and 485 nm (bottom). The first case corresponds to the Mie electric dipole resonance, while the second case to the magnetic one.[16,17] We calculate the contribution of the absorption to the extinction peak and show it in Figure 3d. Both the nanocylinder Mie resonances and the grating condition induce absorption peaks, and a maximum absorption value of ∼50% is predicted. This is in agreement with a recent investigation on superabsorbing free-standing metamaterials, showing that 50% absorption is achieved if the forward-scattered wave is exactly π-delayed with respect to the incident one.[30] In Supplementary Figures S3 and S4 we calculate the dependence of the absorption spectra on the nanocylinder diameter, height, and distance. In Supplementary Figure S5, we demonstrate the condition for enhanced absorption for our 2D metamaterial configuration.

The calculated extinction peaks of Figure 3b are blue-shifted with respect to the experimental ones of Figure 2d. This is due to the fact that the substrate is neglected in the calculations (i.e., the 2D array is free-standing). The effects of the substrate have been already investigated, and they are well-known to determine a red-shift of the resonances and a change in their relative amplitude.[17,30] Moreover, the calculated peaks feature a narrower spectral width and a larger separation between the electric and magnetic resonances. We attribute this to the

DOI: 10.1021/acsphotonics.7b00320
ACS Photonics 2017, 4, 2187−2196

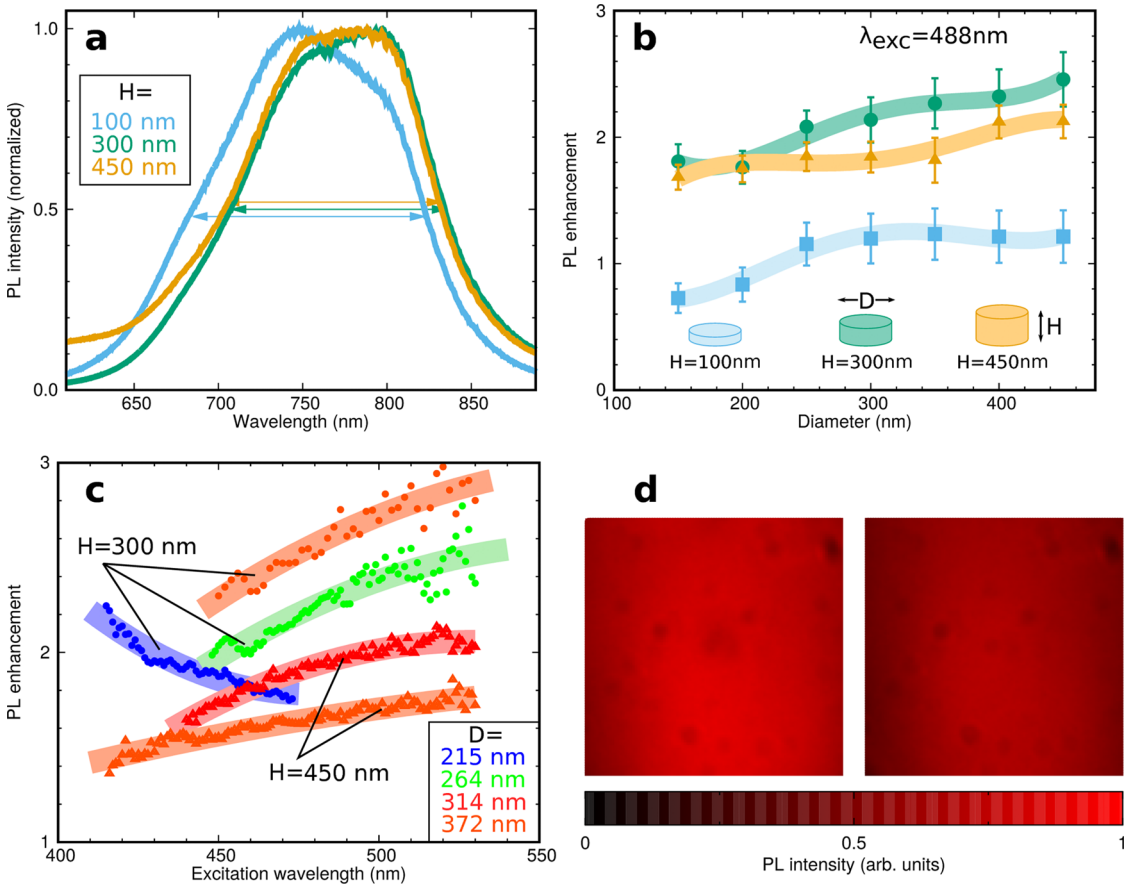

Figure 4. (a) Representative PL spectra of metamaterials with H = 100 nm (cyan), 300 nm (olive-green), and 450 nm (tan) and with D = 215 nm excited at λ_{exc} = 488 nm. (b) PL enhancement as a function of nanocylinder diameter of metamaterials with H = 100 nm (cyan), 300 nm (olive-green), and 450 nm (tan), for λ_{exc} = 488 nm. (c) PLE enhancement for the metamaterial with D = 215 nm (blue), 264 nm (green), 314 nm (red), and 372 nm (orange). Circles are relative to the metamaterials with H = 300 nm; triangles are for H = 450 nm. (d) CCD image (false color) of the PL intensity from the metamaterial with H = 300 nm and D = 372 nm (left) and the reference sample (right).

significant geometrical imperfections of the fabricated nanoscatterers, which are not ideal cylinders (the top and bottom bases have different diameter, the top one is rounded, the sides are not perfectly vertical, and the surface is not smooth). Eventually, we also mention that the effective refractive index n_{eff} used in the calculations is just an approximation of the actual index, since it is derived from a homogenization method. In Supplementary Figures S6 we show a comparison between experimental and calculated extinction spectra, the latter taking into account the substrate and the geometrical imperfections mentioned above.

The comparison between experiments and calculations conclusively confirms the existence of absorption peaks in the investigated 2D Si-NC:SiO_2 metamaterials due to both the nanocylinder Mie resonances and the grating condition. This absorption enhancement in the Si-NCs is expected to produce an increase of their photoluminescence intensity. As a matter of fact, at steady-state excitation the PL intensity I_{PL}, expressed as photon flux, is

$$I_{PL} \propto QY\, N_T\, \sigma I_{exc} \tag{3}$$

where N_T is the number of Si-NCs and I_{exc} is the excitation flux. The absorption cross-section is $\sigma \approx 10^{-15}$ cm^2 under blue excitation, a value comparable with direct-band-gap semiconductor quantum dots.[42,43] We measure the PL spectra, shown in Figure 4a, by exciting the samples with the 488 nm line of an Ar laser. To quantify the effect of the absorption enhancement on the emission, we measure the PL intensity of the metamaterials (for each of the three heights H) and compare it with that of the planar Si-NC:SiO_2 film (of thickness equal to H) used as reference, under the same excitation conditions. We perform these measurements as a function of the nanocylinder size and of the excitation wavelength. The average Si-NC concentration and PL QY are the same for all the samples with the same height H (including the reference), because they are fabricated starting from the same Si:NC:SIO_2 film. However, the total number N_T of emitting Si-NCs in the metamaterials is lower than the reference ($N_{T,ref}/N_{T,meta}$ = AC^{-1}) due to the nanopatterning. Therefore, we define the PL enhancement as

$$PL_{enh} = \frac{I_{PL,meta}}{I_{PL,ref}} \frac{N_{T,ref}}{N_{T,meta}} = \frac{I_{PL,meta}}{I_{PL,ref}} AC^{-1} \tag{4}$$

The PL enhancement is shown in Figure 4b as a function of the nanocylinder diameter, for the three heights H = 100 nm (cyan), 300 nm (olive-green), and 450 nm (tan). For the metamaterial with H = 100 nm, the PL enhancement increases with the diameter, and then it stays constant at a value of ∼1. This simply means that the average PL intensity per Si-NC is equal to that of the reference planar film. Remarkably, for the sample with H = 300 nm, the absolute PL intensity is equal to that of the reference, i.e., $I_{PL,meta} \approx I_{PL,ref}$, despite the lower

DOI: 10.1021/acsphotonics.7b00320
ACS Photonics 2017, 4, 2187−2196

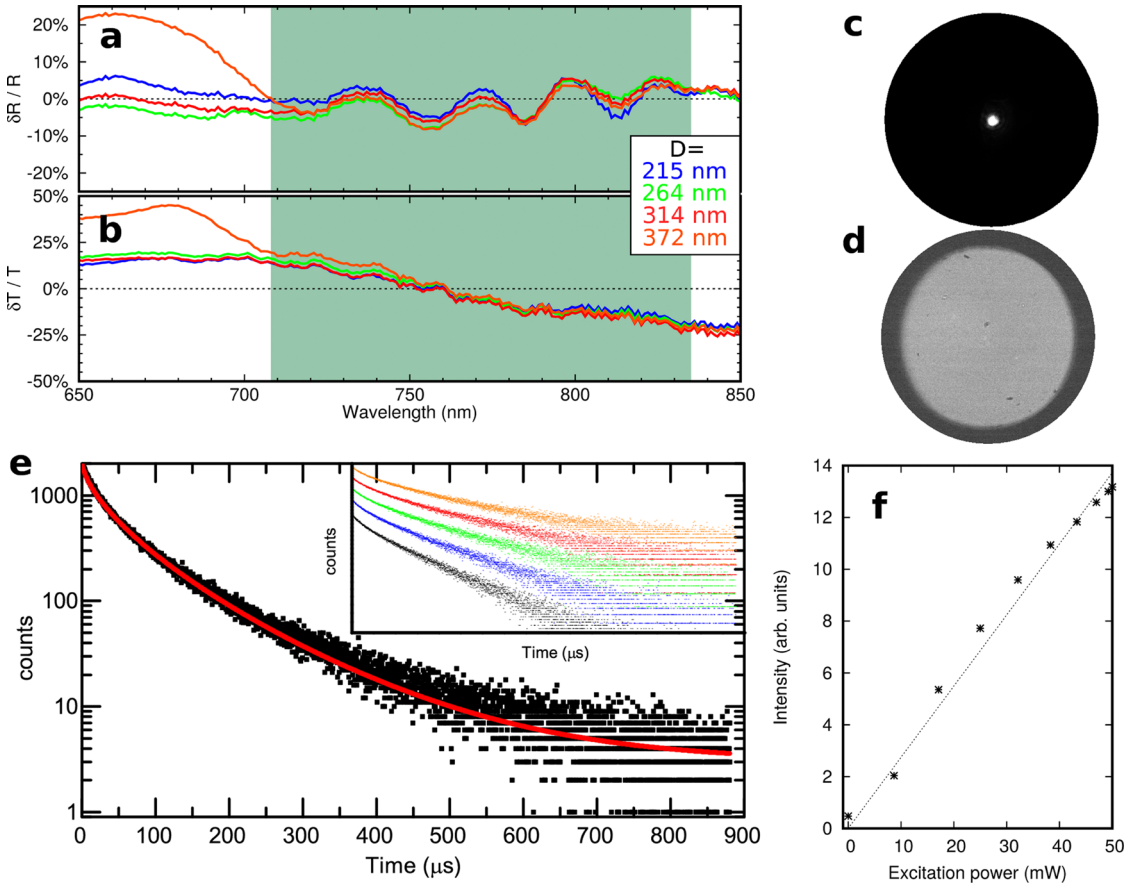

Figure 5. Variation of the measured reflectance (a) and transmittance (b) of the metamaterials with H = 300 nm and D = 215 nm (blue), 264 nm (green), 314 nm (red), and 372 nm (orange), with respect to the reference. The PL full width at half-maximum (fwhm) spectral width is indicated by the sea-green-shaded area. Fourier image of the transmitted light (c) and PL (d) for the metamaterial with H = 300 nm and D = 264 nm. (e) PL intensity time dynamics for the planar reference film (black) and stretched-exponential fit (red). The inset shows the PL decays for the sample metamaterial samples as in panel (a), plotted with an artificial vertical offset, for the sake of clarity. (f) Dependence of the PL intensity on the excitation power for the same sample as in panel (c).

amount of Si-NCs, and the maximum PL enhancement exceeds 2 ($PL_{enh} \approx AC^{-1}$). Eventually, for the sample with H = 450 nm, the PL enhancement slightly decreases from the previous case, confirming again the existence of an optimum nanocylinder height.

In order to confirm the dependence of the absorption enhancement (and therefore of the PL intensity) on the excitation wavelength, we performed photoluminescence excitation (PLE) experiments by scanning the excitation range λ_{exc} = 415−530 nm. The results are shown in Figure 4c, where the circles are relative to the metamaterials with H = 300 nm and the triangles are for H = 450 nm. The metamaterial with H = 300 nm and D = 215 nm (blue line) shows an increase of PL enhancement toward short wavelengths, in proximity of the Mie extinction peak at $\lambda \approx$ 420 nm measured in Figure 2d. Analogously, the sample with D = 264 nm (green line), which features an extinction peak at $\lambda \approx$ 500 nm, shows increased PL toward longer wavelengths up to ∼2.6. The sample with D = 372 nm (orange line) deserves a separate mention, because it features a grating condition in the investigated excitation range, and, interestingly, it shows the highest enhancement value: the $I_{PL\ meta}/I_{PL\ ref}$ ratio is 130% (+30%), and the nominal AC_{meta} is 43%, resulting in an enhancement PL_{enh} = 3.02. This excellent performance, also shown in the PL images of Figure 4d, is easily explained, since the fabrication method determines a small deviation on the nanocylinders' separations (±2 nm), which controls the grating condition, while a much larger error affects their diameter (±10 nm) and shape (bases and surface roughness), reducing the amplitude of the Mie absorption peak, as listed in Supplementary Table S1. The metamaterials with H = 450 nm show analogous trends, but with lower absolute PL enhancement, as already observed in Figure 4b. In order to increase the enhancement factor, we could improve the quality of the nanopatterning, in terms of the nanocylinder diameter, shape, and distance, and by accurately matching the optical impedance of the substrate, as previously discussed in the text. However, while this effort is needed for real applications, it is not strictly necessary to demonstrate the validity of our concept.

In the following, we consider and systematically address all the possible alternative explanations for the observed increase of PL emission, namely, (i) the PL extraction efficiency and (ii) directionality, (iii) the photonic density of states (PDOS), and (iv) the saturation of the Si-NC absorption/emission states. As a matter of fact, the metamaterial nanopattern can modify the PL extraction efficiency and directionality by changing the effective Fresnel reflection and transmission coefficients in the emission spectrum. Moreover, it can modify the PDOS and affect the Si-NC radiative lifetime, due to the Purcell effect.[44,45] Eventually, it can lead to the saturation of the absorption/emission states in the Si-NCs, resulting in an unfair comparison

DOI: 10.1021/acsphotonics.7b00320
ACS Photonics 2017, 4, 2187−2196

between samples and artifacts in the determination of the PL enhancement. We unambiguously prove that these phenomena do not significantly affect the PL intensity of the investigated metamaterial geometries with respect to the reference planar film, and we conclude that the increased absorption efficiency is indeed the dominant process.

A modification of the Fresnel coefficients is simply detectable in the reflection and transmission spectra. Figure 5a and b show the variation of the reflectance $\frac{\delta R(\lambda)}{R(\lambda)}$ and of the transmittance $\frac{\delta T(\lambda)}{T(\lambda)}$, respectively, for the metamaterial samples with respect to the unpatterned film at normal incidence. For all samples, the Mie resonances and the grating conditions are far from the emission spectrum, indicated by the sea-green-shaded area. The maximum values of $\left|\frac{\delta R(\lambda)}{R(\lambda)}\right|$ and $\left|\frac{\delta T(\lambda)}{T(\lambda)}\right|$ are 8% at λ = 758 nm and 22% at λ = 832 nm, respectively, while the average across the emission spectrum is <2% for both. For each wavelength, we quantify the variation of PL intensity due to changes of R and T by using a first-order approximation: $\left.\frac{\delta I_{PL,s}(\lambda)}{I_{PL,s}(\lambda)}\right|_R = \frac{\delta R(\lambda)}{R(\lambda)}$ and $\left.\frac{\delta I_{PL,s}(\lambda)}{I_{PL,s}(\lambda)}\right|_T = \frac{\delta T(\lambda)}{T(\lambda)}$. By considering that the integrated PL intensity is $I_{PL} = \int I_{PL,s}(\lambda)\, d\lambda$, we find that the overall change in PL intensity is only $\left|\frac{\delta I_{PL}}{I_{PL}}\right|_R$ < 2% and $\left|\frac{\delta I_{PL}}{I_{PL}}\right|_T$ < 3%. Therefore, the PL extraction efficiency is approximately the same for the metamaterial and the reference samples.

To directly exclude any change in the PL directionality, we perform Fourier (or k-space) microscopy of the PL intensity. This technique is based on capturing the Fourier plane image formed in the back focal plane of a high-NA objective, which contains the k-space information on the radiative field. For all the samples, including the reference, the Fourier image is homogeneous, which indicates an isotropic PL emission. Here we focus on one representative metamaterial sample with H = 300 nm and D = 264 nm, and we first report in Figure 5c the Fourier image of the transmitted light. It only shows the 0th-order central spot, which simply confirms that the metamaterial is subwavelength at the excitation wavelength. The Fourier image of PL is displayed in Figure 5d, and it shows isotropic emission. Therefore, we can exclude any effect of the PL angular dependence on the observed PL enhancement.

Furthermore, a change in the PDOS in the metamaterial samples would significantly affect the PL spectrum and lifetime. On the contrary, our measurements indicate that they do not change with the nanocylinder diameter, and they are equal to those of the reference sample. Specifically, the average PL lifetime is ~45 ± 2 μs, as obtained by fitting the decay with a stretched-exponential function. In Figure 5e, we show the PL time dynamics of the reference sample (black) and of the metamaterial samples with the highest PL enhancement (H = 300 nm and D = 215, 264, and 372 nm). Therefore, we can exclude any effect of the PDOS on the observed PL enhancement. Eventually, Figure 5f shows the dependence of the PL intensity on the excitation power for the representative sample with H = 300 nm and D = 264 nm, which clearly indicates that all the samples were characterized in the linear regime, far from the saturation of the Si-NCs. Therefore, we can safely attribute the increased PL in the metamaterial samples exclusively to the enhancement of the absorption at the excitation wavelength. This result was remarkably achieved without affecting the transmission/reflection properties in the emission spectrum. Moreover, the emission properties in terms of angular pattern, lifetime, and spectral shape are approximately the same as the planar sample without nanocylinders.

CONCLUSIONS

In conclusion, we have successfully integrated quantum-confined Si-NCs into SiO_2 nanocylinders, arranged into a 2D metamaterial. This hierarchical metamaterial inherits the optical and electronic properties of its building blocks and shows boosted performances over the individual components. We have experimentally detected the occurrence of extinction peaks related to dipole Mie resonances in the nanocylinders and to the grating condition, which can be tailored throughout the visible spectrum. Both of them induce spectrally selective enhancement of the absorption, as predicted by our rigorous calculations. The Si-NCs experience increased excitation and, as a consequence, exhibit a more intense light emission. Remarkably, our experiments show that the best-performing metamaterial features higher light emission than a planar film without nanopatterning, despite the reduced amount of Si-NCs. The metamaterial design principles described in this work are applicable to any QD semiconductor and to other emitters such as rare-earth ions and organic molecules. The specific implementation investigated in this work is completely based on Si, it is fully compatible with CMOS technology, and it can be integrated with Si solar cells for spectral shaping purposes. We envision the application of this approach to photovoltaics, photocatalysis, and photosynthesis.

ASSOCIATED CONTENT

Supporting Information

The Supporting Information is available free of charge on the ACS Publications website at DOI: 10.1021/acsphotonics.7b00320.

Effective refractive index of the Si-NC:SiO_2 medium, metamaterial fabrication process, list of samples, calculated absorption spectra as a function of the metamaterial geometry, condition for enhanced absorption in 2D metamaterials, and calculated extinction spectra taking into account the substrate and the geometrical imperfections (PDF)

AUTHOR INFORMATION

Corresponding Author

*E-mail: a.capretti@uva.nl.

ORCID

Antonio Capretti: 0000-0002-6705-9280

Tom Gregorkiewicz: 0000-0003-2092-8378

Author Contributions

A.C. and T.G. conceived the idea and designed the experiments. A.C. performed the nanolithography process, the optical experiments, the electromagnetic calculations, the data analysis and wrote the manuscript. A.L. fabricated the planar Si-NC:SiO_2 films and contributed to the PLE experiments and to the SEM analysis. T.G. supervised the overall project. All authors participated in discussion and read and approved the final version of the manuscript.

Notes

The authors declare no competing financial interest.

DOI: 10.1021/acsphotonics.7b00320
ACS Photonics 2017, 4, 2187−2196

■ ACKNOWLEDGMENTS

The authors acknowledge Prof. Femius Koenderink for facilitating the measurement of the metamaterial 0th-order transmittance, reflectance, and the Fourier microscopy. The authors acknowledge financial support from Solardam (within the UvA-VU Amsterdam Academic Alliance Fund) and from the Nederlandse Organisatie voor Wetenschappelijk Onderzoek (TTW Domain, formerly STW).

■ REFERENCES

(1) Konstantatos, G.; Sargent, E. H. Nanostructured Materials for Photon Detection. *Nat. Nanotechnol.* **2010**, *5*, 391−400.
(2) Shirasaki, Y.; Supran, G. J.; Bawendi, M. G.; Bulović, V. Emergence of Colloidal Quantum-Dot Light-Emitting Technologies. *Nat. Photonics* **2013**, *7*, 13−23.
(3) Priolo, F.; Gregorkiewicz, T.; Galli, M.; Krauss, T. F. Silicon Nanostructures for Photonics and Photovoltaics. *Nat. Nanotechnol.* **2014**, *9*, 19−32.
(4) Tanaka, K.; Plum, E.; Ou, J. Y.; Uchino, T.; Zheludev, N. I. Multifold Enhancement of Quantum Dot Luminescence in Plasmonic Metamaterials. *Phys. Rev. Lett.* **2010**, *105*, 1−4.
(5) Jin, Y.; Gao, X. Plasmonic Fluorescent Quantum Dots. *Nat. Nanotechnol.* **2009**, *4*, 571−576.
(6) Muskens, O. L.; Giannini, V.; Sanchez-Gil, J. A.; Gómez Rivas, J.; Sánchez-Gil, J. A.; Gómez Rivas, J. Strong Enhancement of the Radiative Decay Rate of Emitters by Single Plasmonic Nanoantennas. *Nano Lett.* **2007**, *7*, 2871−2875.
(7) Soukoulis, C. M.; Wegener, M. Past Achievements and Future Challenges in the Development of Three-Dimensional Photonic Metamaterials. *Nat. Photonics* **2011**, *5*, 523−530.
(8) Jahani, S.; Jacob, Z. All-Dielectric Metamaterials. *Nat. Nanotechnol.* **2016**, *11*, 23−36.
(9) Kuznetsov, A. I.; Miroshnichenko, A. E.; Brongersma, M. L.; Kivshar, Y. S.; Lukyanchuk, B. Optically Resonant Dielectric Nanostructures. *Science (Washington, DC, U. S.)* **2016**, *354*, aag2472.
(10) Evlyukhin, A. B.; Novikov, S. M.; Zywietz, U.; Eriksen, R. L.; Reinhardt, C.; Bozhevolnyi, S. I.; Chichkov, B. N. Demonstration of Magnetic Dipole Resonances of Dielectric Nanospheres in the Visible Region. *Nano Lett.* **2012**, *12*, 3749−3755.
(11) Kuznetsov, A. I.; Miroshnichenko, A. E.; Fu, Y. H.; Zhang, J.; Luk'yanchuk, B. Magnetic Light. *Sci. Rep.* **2012**, *2*, 492.
(12) Zhao, Q.; Zhou, J.; Zhang, F.; Lippens, D. Mie Resonance-Based Dielectric Metamaterials. *Mater. Today* **2009**, *12*, 60−69.
(13) Fu, Y. H.; Kuznetsov, A. I.; Miroshnichenko, A. E.; Yu, Y. F.; Luk'yanchuk, B. Directional Visible Light Scattering by Silicon Nanoparticles. *Nat. Commun.* **2013**, *4*, 1527.
(14) Nieto-Vesperinas, M.; Gomez-Medina, R.; Saenz, J. J. Angle-Suppressed Scattering and Optical Forces on Submicrometer Dielectric Particles. *J. Opt. Soc. Am. A* **2011**, *28*, 54−60.
(15) Ginn, J. C.; Brener, I.; Peters, D. W.; Wendt, J. R.; Stevens, J. O.; Hines, P. F.; Basilio, L. I.; Warne, L. K.; Ihlefeld, J. F.; Clem, P. G.; et al. Realizing Optical Magnetism from Dielectric Metamaterials. *Phys. Rev. Lett.* **2012**, *108*, 1−5.
(16) Staude, I.; Miroshnichenko, A. E.; Decker, M.; Fofang, N. T.; Liu, S.; Gonzales, E.; Dominguez, J.; Luk, T. S.; Neshev, D. N.; Brener, I.; et al. Tailoring Directional Scattering through Magnetic and Electric Resonances in Subwavelength Silicon Nanodisks. *ACS Nano* **2013**, *7*, 7824−7832.
(17) van de Groep, J.; Polman, A.; Van de Groep, J.; Polman, A.; van de Groep, J.; Polman, A. Designing Dielectric Resonators on Substrates: Combining Magnetic and Electric Resonances. *Opt. Express* **2013**, *21*, 1253−1257.
(18) Shcherbakov, M. R.; Vabishchevich, P. P.; Shorokhov, A. S.; Chong, K. E.; Choi, D. Y.; Staude, I.; Miroshnichenko, A. E.; Neshev, D. N.; Fedyanin, A. A.; Kivshar, Y. S. Ultrafast All-Optical Switching with Magnetic Resonances in Nonlinear Dielectric Nanostructures. *Nano Lett.* **2015**, *15*, 6985−6990.
(19) Lin, D.; Fan, P.; Hasman, E.; Brongersma, M. L. Dielectric Gradient Metasurface Optical Elements. *Science (Washington, DC, U. S.)* **2014**, *345*, 298−302.
(20) Aieta, F.; Kats, M. A.; Genevet, P.; Capasso, F. Multiwavelength Achromatic Metasurfaces by Dispersive Phase Compensation. *Science (Washington, DC, U. S.)* **2015**, *347*, 1342−1345.
(21) Spinelli, P.; Verschuuren, M.; Polman, A. Broadband Omnidirectional Antireflection Coating Based on Subwavelength Surface Mie Resonators. *Nat. Commun.* **2012**, *3*, 692.
(22) Spinelli, P.; Polman, A. Light Trapping in Thin Crystalline Si Solar Cells Using Surface Mie Scatterers. *IEEE J. Photovoltaics* **2014**, *4*, 554−559.
(23) Trupke, T.; Green, M. A.; Würfel, P. Improving Solar Cell Efficiencies by down-Conversion of High-Energy Photons. *J. Appl. Phys.* **2002**, *92*, 1668−1674.
(24) Kovalev, D.; Heckler, H.; Polisski, G.; Diener, J.; Koch, F. Optical Properties of Silicon Nanocrystals. *Opt. Mater.***2001**, *17*, 35−4010.1016/S0925-3467(01)00017-9.
(25) Timmerman, D.; Izeddin, I.; Stallinga, P.; Yassievich, I. N.; Gregorkiewicz, T. Space-Separated Quantum Cutting with Silicon Nanocrystals for Photovoltaic Applications. *Nat. Photonics* **2008**, *2*, 105−109.
(26) Trinh, M. T.; Limpens, R.; de Boer, W. D. a. M.; Schins, J. M.; Siebbeles, L. D. a.; Gregorkiewicz, T. Direct Generation of Multiple Excitons in Adjacent Silicon Nanocrystals Revealed by Induced Absorption. *Nat. Photonics* **2012**, *6*, 316−321.
(27) Strümpel, C.; McCann, M.; Beaucarne, G.; Arkhipov, V.; Slaoui, A.; Švrček, V.; del Cañizo, C.; Tobias, I. Modifying the Solar Spectrum to Enhance Silicon Solar Cell Efficiency-An Overview of Available Materials. *Sol. Energy Mater. Sol. Cells* **2007**, *91*, 238−249.
(28) Švrček, V.; Slaoui, A.; Muller, J. C. Silicon Nanocrystals as Light Converter for Solar Cells. *Thin Solid Films* **2004**, *451*−*452*, 384−388.
(29) Yuan, Z.; Pucker, G.; Marconi, A.; Sgrignuoli, F.; Anopchenko, A.; Jestin, Y.; Ferrario, L.; Bellutti, P.; Pavesi, L. Silicon Nanocrystals as a Photoluminescence down Shifter for Solar Cells. *Sol. Energy Mater. Sol. Cells* **2011**, *95*, 1224−1227.
(30) Kim, S. J.; Park, J.; Esfandyarpour, M.; Pecora, E. F.; Kik, P. G.; Brongersma, M. L. Superabsorbing, Artificial Metal Films Constructed from Semiconductor Nanoantennas. *Nano Lett.* **2016**, *16*, 3801−3808.
(31) Limpens, R.; Luxembourg, S. L.; Weeber, A. W.; Gregorkiewicz, T. Emission Efficiency Limit of Si Nanocrystals. *Sci. Rep.* **2016**, *6*, 19566.
(32) Dohnalová, K.; Gregorkiewicz, T.; Kůsová, K. Silicon Quantum Dots: Surface Matters. *J. Phys.: Condens. Matter* **2014**, *26*, 173201.
(33) Khriachtchev, L.; Nikitin, T.; Oton, C. J.; Velagapudi, R.; Sainio, J.; Lahtinen, J.; Novikov, S. Optical Properties of Silicon Nanocrystals in Silica: Results from Spectral Filtering Effect, M-Line Technique, and X-Ray Photoelectron Spectroscopy. *J. Appl. Phys.* **2008**, *104*, 10431610.1063/1.3010304.
(34) Nikitin, T.; Velagapudi, R.; Sainio, J.; Lahtinen, J.; Räsänen, M.; Novikov, S.; Khriachtchev, L. Optical and Structural Properties of SiOx Films Grown by Molecular Beam Deposition: Effect of the Si Concentration and Annealing Temperature. *J. Appl. Phys.* **2012**, *112*, 09431610.1063/1.4764893.
(35) Fujiwara, H. *Principles of Spectroscopic Ellipsometry*; Wiley, 2007.
(36) Timmerman, D.; Valenta, J.; Dohnalová, K.; de Boer, W. D. a. M.; Gregorkiewicz, T. Step-like Enhancement of Luminescence Quantum Yield of Silicon Nanocrystals. *Nat. Nanotechnol.* **2011**, *6*, 710−713.
(37) Yi, L. X.; Heitmann, J.; Scholz, R.; Zacharias, M. Phase Separation of Thin SiO Layers in Amorphous SiO/SiO 2 Superlattices during Annealing. *J. Phys.: Condens. Matter* **2003**, *15*, S2887−S2895.
(38) Miura, S.; Nakamura, T.; Fujii, M.; Inui, M.; Hayashi, S. Size Dependence of Photoluminescence Quantum Efficiency of Si Nanocrystals. *Phys. Rev. B: Condens. Matter Mater. Phys.* **2006**, *73*, 245333.
(39) Greben, M.; Valenta, J. Note: On the Choice of the Appropriate Excitation-Pulse-Length for Assessment of Slow Luminescence Decays. *Rev. Sci. Instrum.* **2016**, *87*.12610110.1063/1.4971368

DOI: 10.1021/acsphotonics.7b00320
ACS Photonics 2017, 4, 2187−2196

(40) Doicu, A.; Wriedt, T.; Eremin, Y. A. *Light Scattering by Systems of Particles*; Springer, 2006; Vol. *124*.
(41) Liu, V.; Fan, S. S 4: A Free Electromagnetic Solver for Layered Periodic Structures. *Comput. Phys. Commun.* **2012**, *183*, 2233−2244.
(42) Valenta, J.; Greben, M.; Remeš, Z.; Gutsch, S.; Hiller, D.; Zacharias, M. Determination of Absorption Cross-Section of Si Nanocrystals by Two Independent Methods Based on Either Absorption or Luminescence. *Appl. Phys. Lett.* **2016**, *108*, 23102.
(43) Leatherdale, C. A.; Woo, W. K.; Mikulec, F. V.; Bawendi, M. G. On the Absorption Cross Section of CdSe Nanocrystal Quantum Dots. *J. Phys. Chem. B* **2002**, *106*, 7619−7622.
(44) Novotny, L.; Hecht, B. *Principle of Nano-Optics*; Cambridge University Press, 2006; Vol. *1*.
(45) Wang, Y.; Sugimoto, H.; Inampudi, S.; Capretti, A.; Fujii, M.; Dal Negro, L. Broadband Enhancement of Local Density of States Using Silicon-Compatible Hyperbolic Metamaterials. *Appl. Phys. Lett.* **2015**, *106*, 1−5.

DOI: 10.1021/acsphotonics.7b00320
ACS Photonics 2017, 4, 2187−2196